Master's Thesis

Enhancement in device performance via modification of hole transport layer in organic photovoltaics

Donghwan Koo

Department of Energy Engineering

(Energy Engineering)

Graduate School of UNIST

2019

Enhancement in device performance via modification of hole transport layer in organic photovoltaics

Donghwan Koo

Department of Energy Engineering

(Energy Engineering)

Graduate School of UNIST

Enhancement in device performance via modification of hole transport layer in organic photovoltaics

A thesis/dissertation
submitted to the Graduate School of UNIST
in partial fulfillment of the
requirements for the degree of
Master of Science

Donghwan Koo

01/10/2019
Approved by

Advisor
Hyesung Park

Enhancement in device performance via modification of hole transport layer in organic photovoltaics

Donghwan Koo

This certifies that the thesis/dissertation of Donghwan Koo is approved.

01/10/2019

signature

Advisor: Hyesung Park

signature

Changduk Yang: Thesis Committee Member #1

signature

Jongnam Park: Thesis Committee Member #2

Abstract

Transition metal dichalcogenides (TMDs) have received significant attention because of their potentials for replacing or modifying the existing charge transporting materials in organic solar cells (OSCs) with their unique crystalline structure and desirable electrical properties. Poly(3,4-ethylene dioxythiophene):poly(styrene sulfonate) (PEDOT:PSS) has been considered as the representative hole transporting material owing to its notable optical transmittance, electrical conductivity, and solution-processability. In this study, we provide a facile method to introduce liquid-phase exfoliated TMD, tungsten diselenide (WSe_2), as the device performance enhancer in OSCs. Implementation of WSe_2 into PEDOT:PSS without significant change to the surface morphology mediates effective charge transport in the completed device. The phase separation of PEDOT and PSS induced by the WSe_2 provides a conductivity enhancement in the modified hole transport layer (HTL), which contributes to the increase of hole mobility and decrease of charge recombination loss in the OSCs, resulting in the improvement of power conversion efficiency from 7.3% to 8.5% for pristine and modified HTL devices, respectively. These results provide a simple strategy for the enhancement of device performance in OSCs, demonstrating their promising potential in the application of TMDs for next-generation energy harvesting devices.

List of Figures

List of Table

I. Introduction

1.1 Advantages of Organic Solar Cells

Solar cells, which are an eco-friendly energy source that convert solar energy into electrical energy and has abundant sources are attracting much attention as an alternative energy source for substitution of existing fossil fuel which is one of the main factors for severe global warming. The photovoltaic devices can be simply classified into several types depending on the device structures and the materials for generating charge carriers. Among the many kinds of solar cells, the organic solar cells which is consist of photoactive layer and charge transport layer (CTL) and two electrodes are attracting much attention for next-generation photovoltaics owing to their advantages such as solution processabilities, cost-effective materials and fabrication process, applicability to commercialized device with mechanical flexibility of organic materials, the possibility of large scaled device via roll-to-roll process[1-6] and power conversion efficiency (PCE) over 13%. Recently, tremendous studies are focusing on commercial perspectives such as the efficiency, stability and flexibility of OSCs for next-generation energy harvesting devices.

1.2 Principle and Characterization of Solar Cells

The efficiency of the completed device is affected by various parameters such as short-circuit current (I_{sc}), open-circuit voltage (V_{oc}) and fill factor (FF). The I_{sc} is the maximum current when the voltage of the solar cell is zero which is originated from generation and collection of photogenerated charge carriers. The I_{sc} is influenced by various factors, such as the optical properties, the area of the solar cell, the amount of absorbed incident light and the collection probability. The V_{oc} is a maximum voltage of the device which is amount of forward bias that occurs when the current is zero and can be obtained by followed equation:

$$V_{OC} = \frac{nkT}{q} \ln\left[\frac{I_{SC}}{I_0} + 1\right]$$

It can be seen that V_{oc} relies on I_{sc} and the saturation current (I_0) of the device through the above equation. Since I_0 depends on charge recombination quantity of recombination in completed device. The FF is another important parameter which determine the maximum power of the device. FF is the ratio of maximum power to actual value and is a parameter that can evaluates how ideal the device is fabricated.

$$\mathrm{FF} = \frac{V_{max}J_{max}}{V_{OC}J_{SC}}$$

And the solar cell efficiency (η) is defined as equation

$$\eta = \frac{J_{SC} V_{OC} FF}{P_{in}}$$

And stability of the device is influenced by the diffusion of electrode into other layer, moisture, temperature, incident light and stability of crystallization of polymers. With various parameters, improved device performance has been realized by primarily devoting on some aspects: Development of alternative conductive electrodes to indium tin oxide (ITO) or other metal electrodes;[7-9] substitution and modification of existing charge transport layers;[10,11] addition of novel additives into the photoactive and charge transport layer for flexible, stable and efficient devices.[12-14]

1.3 Characterization of CTL

Among each layer in OSCs, the photoactive layer can be considered as the most important part as they generate the charge carriers via photovoltaic effect. However, in the absence of the charge transport layer, the recombination of charge carriers occurs at the interface between photoactive layer and electrode due to large difference in energy level while the photogenerated charge carriers reach counter electrode to produce electrical energy which resulting in decreased device performances. Thus, as shown in Figure 1.1, to suppress the charge recombination and degradation of the device performance, charge transport layer was introduced into interface between electrode and photoactive layer. With the suitable energy level or wide bandgap of charge transport layer induces the improved device efficiency along with the decline of charge recombination. From this perspective, charge transport layer plays crucial roles as much as photoactive layer for efficient devices and still very much of research is being studying to develop better CTLs and apply them into solar cell devices.

1.4 Properties of PEDOT:PSS

For hole transport layer (HTL), the Poly(3,4-ethylene dioxythiophene):poly(styrene sulfonate) (PEDOT:PSS) has been widely used as the representative hole transport materials in OSCs owing to its outstanding electrical and optical properties with solution processability, thermal stability and mechanical flexibility. The PEDOT:PSS is consist of two polymer, the conducting PEDOT and insulating PSS. The PSS chain attached to PEDOT with very weak coulombic interaction to disperse the conducting PEDOT in aqueous solvent and surround the PEDOT leading to disturb the connection between the PEDOT chains (Figure 1.2). However, with the insulating property of PSS, the conductivity of PEDOT:PSS film is still insufficient.[15] Thus, limited hole transporting ability within the pristine PEDOT:PSS results in reduced performance of the completed devices along with the charge accumulation at the interfaces which resulting in charge recombination. To overcome the limitations,

several strategies have been investigated to improve the hole transporting ability of PEDOT:PSS including doping with additives and post-treatment by organic solvents.[16-18] These strategies showed enhanced conductivity along with better charge transport abilities of PEDOT:PSS films and resulted in improved device performances due to increased current density (J_{SC}).

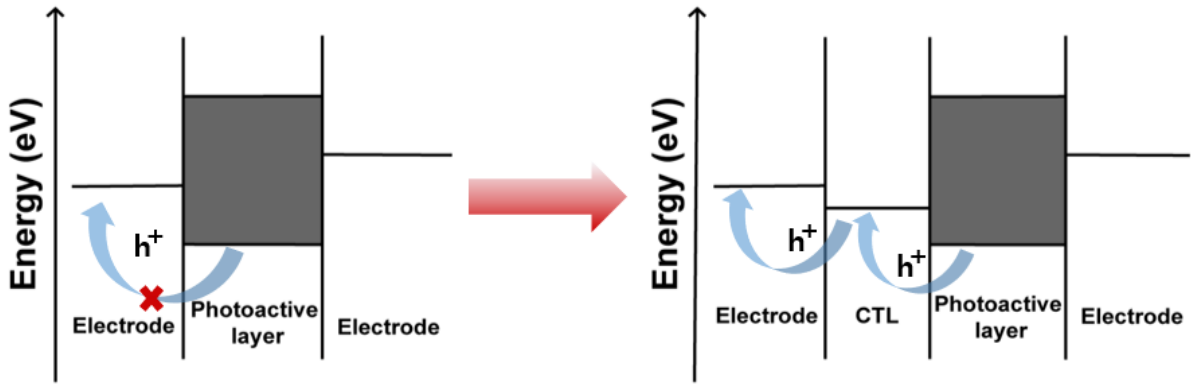

Figure 1.1 The hole trasnfer dynamic of with and without CTL.

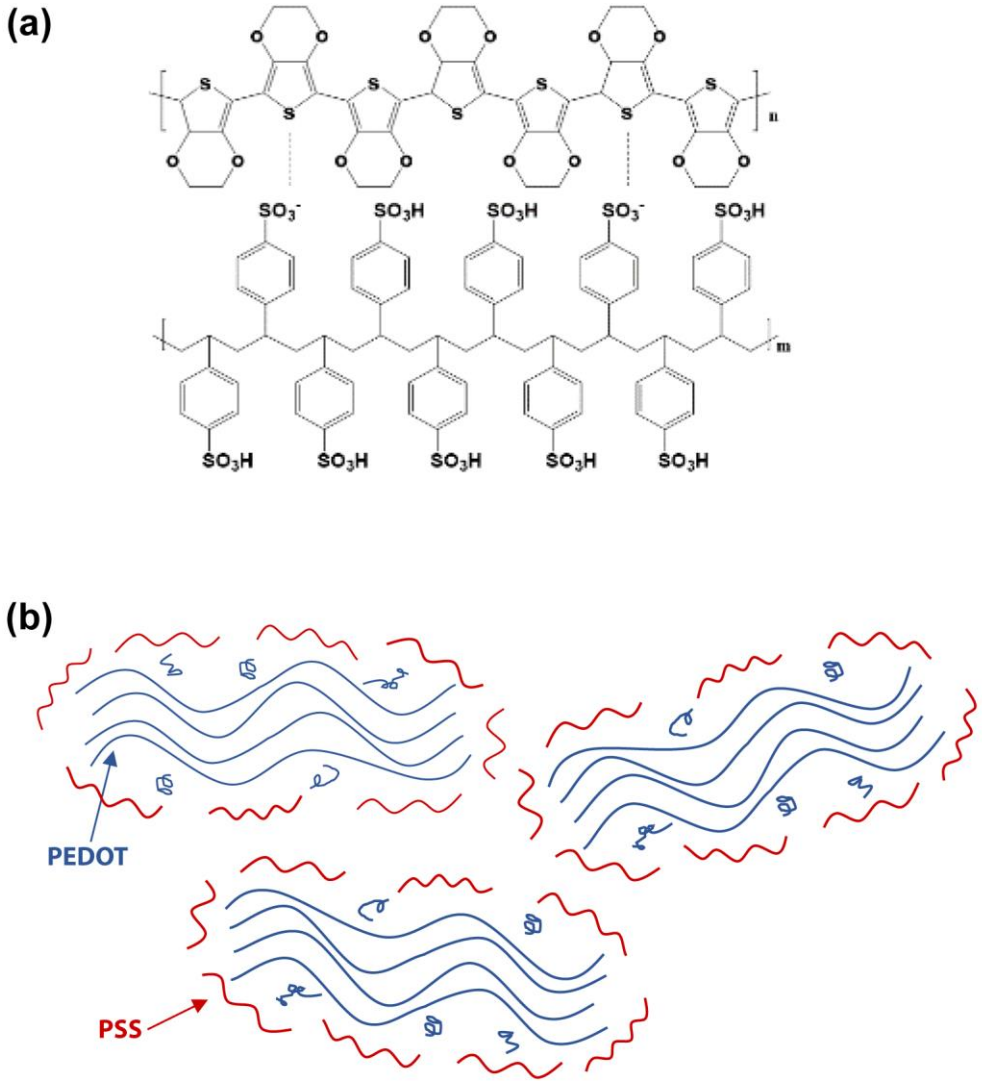

Figure 1.2 (a) The chemical structure and (b) morphology of PEDOT:PSS.

1.5 Properties of TMDs

Two-dimensional materials, such as graphene derivatives and transition metal dichalcogenides (TMDs), have drawn a great deal of attention in photovoltaic field with their unique optical and electrical properties.[19-22] Since the bulk form of two-dimensional materials can be readily exfoliated into few layers through facile solution processed method due to weak van der Walls forces between the layers, flakes show great potential use in photovoltaic devices via facile depositing process such as spin coating or spray coatings which can be applied to roll-to-roll process for large-scaled devices.[23-25] Recently, a number of studies have been suggested for using liquid-phase exfoliated TMDs as an additive in photoactive layer which improve the charge carrier dynamics and charge transport layer for OSCs owing to their semiconducting property with direct bandgap. With their remarkable optoelectrical properties, they exhibit improved device performances such as enhanced device efficiency and stability. However, due to the flake nature of exfoliated materials, formation of a uniform surface morphology is considered as the most important part in solution processed devices.[26,27] To avoid the deterioration of surface morphology, several strategies have been suggested such as repeated spin coating or concentration controls of flake dispersion.

In this study, we introduced TMDs into widely used HTL, PEDOT:PSS, to fabricate efficient OSCs by modifying PEDOT:PSS via facile method. The little amount of liquid-phase exfoliated two-dimensional layered tungsten diselenide (WSe_2) nanocrystals in 2H phase crystalline structure were introduced into the PEDOT:PSS solution with forming a stable dispersion. With the little amount of addition of WSe_2, the WSe_2-modified PEDOT:PSS shows homogeneous film without considerable changes in the uniformity of surface morphology. The improved device performances were mainly originated from the increased conductivity and hole transporting ability of WSe_2-mediated PEDOT:PSS. Increased charge transporting performance was corroborated by the hole mobility and photoluminescence characterization, also. The changes in electrical property of mediated PEDOT:PSS comes from the phase separation between PEDOT and PSS and formation of PEDOT cluster which can provide efficient pathway for the photogenerated charge carriers. The phase separation was induced by negatively charged surface of WSe_2 flakes which weaken the coulombic interaction between PEDOT and PSS. The improved hole transporting ability of modified HTL resulted in notable enhancement in the device performance, with the enhancement in PCE from 7.3% to 8.5% from pristine and mediated HTL, respectively. This approach provide a facile strategy to improve the charge transporting ability of PEDOT:PSS in OSCs along with the increased device performance and provide the potential application of TMDs into various optoelectronic devices beyond the solar cells.

II. Results & Discussion

2.1 Liquid-phase Exfoliation and Optimization of WSe_2 dispersion

WSe_2 flakes was synthesized from liquid-phase exfoliation method and dispersed in a deionized water and isopropanol mixture for modulating the surface tension difference between WSe_2 flakes and solvent to obtain high dispersibility of WSe_2 dispersion. As shown in Figure 2.1, WSe_2 flakes were dispersed in various ration between water and IPA to acquire the most stable dispersion and highest concentration of WSe_2, after exfoliated and centrifuged. By increasing the ratio of IPA in co-solvent, we found that WSe_2 flakes shows the highest dispersibility at the ratio of water and IPA of 4:6, and the highest concentration, 0.9 mg/ml, of WSe_2 dispersion was obtained.

After, the UV-vis-NIR measurement of WSe_2 dispersion with various mixture ratio were performed to precisely find out the most stable dispersion (Figure 2.2). The intensity of absorption peak indicates that the relative amount of WSe_2 flakes in dispersion. The intensity of 4:6 mixing ratio shows the highest peak compare to others which implies that the WSe_2 flakes has the highest dispersibility in co-solvent with the ratio of 4:6 and thus has the highest concentration.

2.2 Characterization of as-exfoliated WSe_2

To characterize the as-exfoliated WSe_2 flakes, the optical analysis was investigated. As shown in Figure 2.3, the UV-vis-NIR of WSe_2 flakes result exhibits the two distinctive absorption peaks at 755 nm and 600 nm for A and B exciton of WSe_2. With two inherent absorption peaks, we could verify that the exfoliated WSe_2 has semiconducting 2H phase crystalline structure which indicate that the crystal structure of WSe_2 did not show any changes as the WSe_2 was exfoliated via simple sonication without using other materials such as Li, Na and K which is used for changing the crystalline structure and electrical properties.[28,29]

Raman spectroscopy was conducted to further examine the nature of 2H phase crystalline WSe_2 (Figure 2.4). Through the two dominant peaks at 251 and 256 cm^{-1} which is account for in-plane E^1_{2g} and out-of-plane A_{1g} vibration modes of 2H-WSe2, respectively, we further verify that the WSe_2 flakes was exfoliated without any changes in electrical properties.[30,31]

With the flake nature of as-exfoliated WSe_2 flakes, the morphology of WSe_2 flakes could affect the uniformity of HTL films along with device performances, the surface morphology of WSe_2 flakes were investigated with atomic microscopy (AFM). As shown in Figure 2.5, we observed that the thickness of as-exfoliated WSe_2 flakes was less than 2 nm with the lateral size of 100 to 200 nm indicating that the bulk state of WSe_2 powder was effectively exfoliated into few layers in thickness and WSe_2 flakes

will have semiconducting properties with direct bandgap. From the surface morphology of spin coated WSe_2 flakes results, we could anticipate that the incorporating the WSe_2 flakes into PEDOT:PSS will not have a significant adverse effect on device performance.

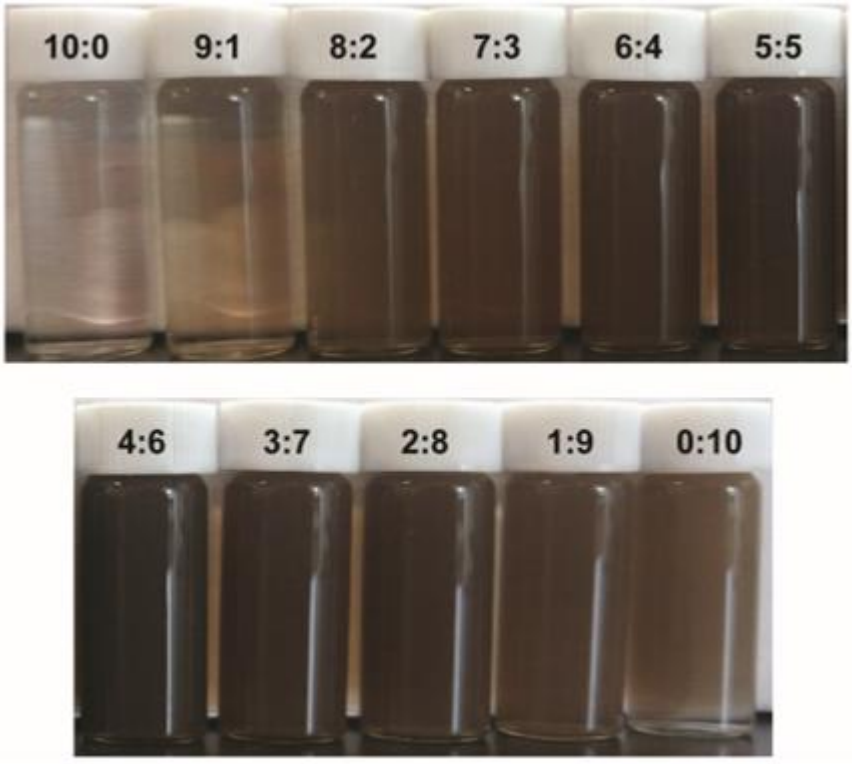

Figure 2.1 Digital image of exfoliated and centrifuged WSe_2 dispersion with varying volume ratio of co-solvent (water:IPA, v/v).

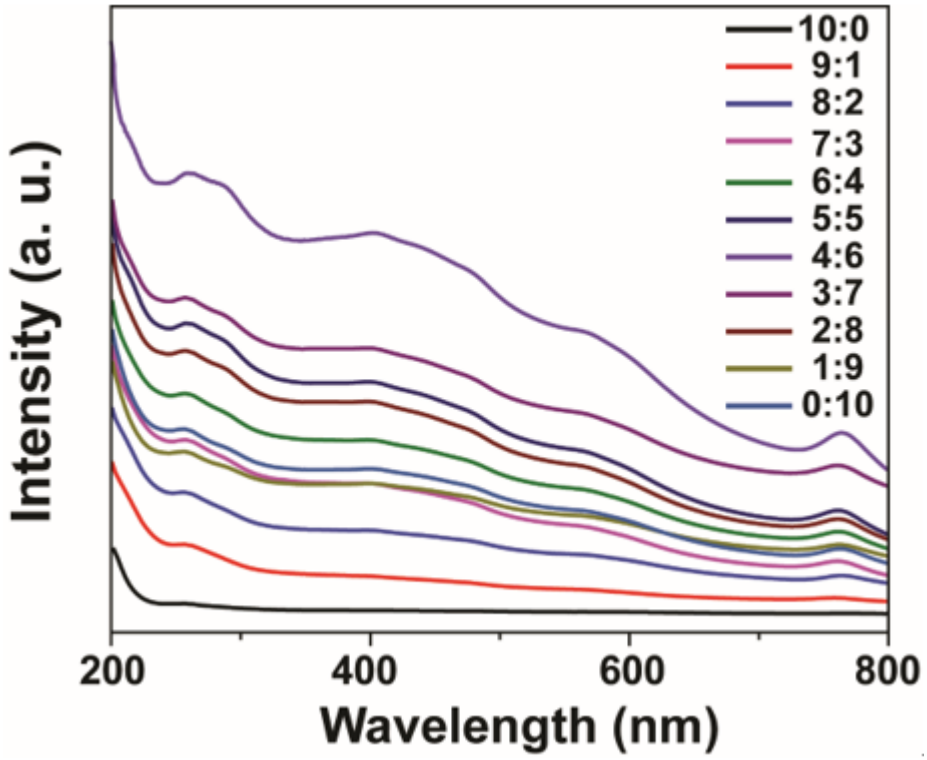

Figure 2.2 UV-vis-NIR absorption spectra of exfoliated and centrifuged WSe_2 dispersion with varying volume ratio of co-solvent (water:IPA, v/v).

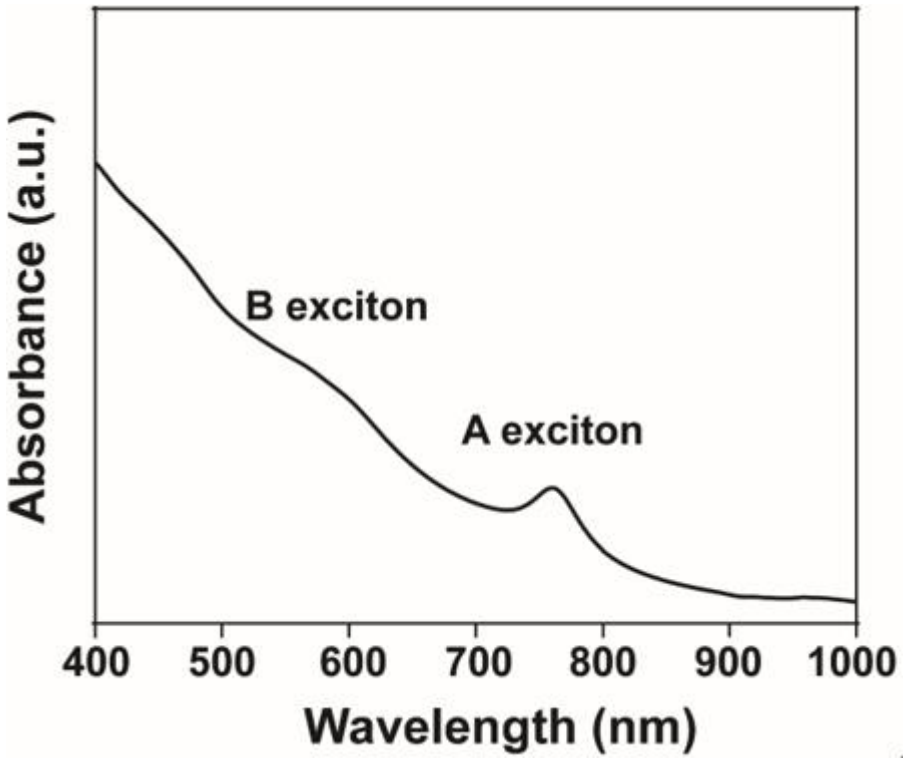

Figure 2.3 Absorption spectrum of exfoliated WSe_2 solution.

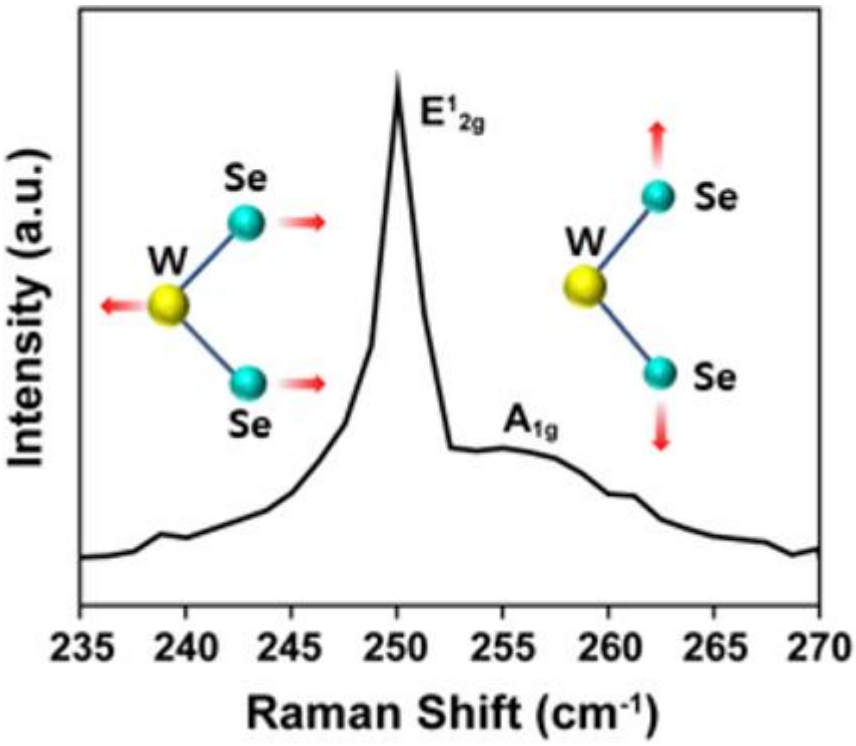

Figure 2.4 Raman spectrum of WSe_2 flakes on SiO_2 substrate.

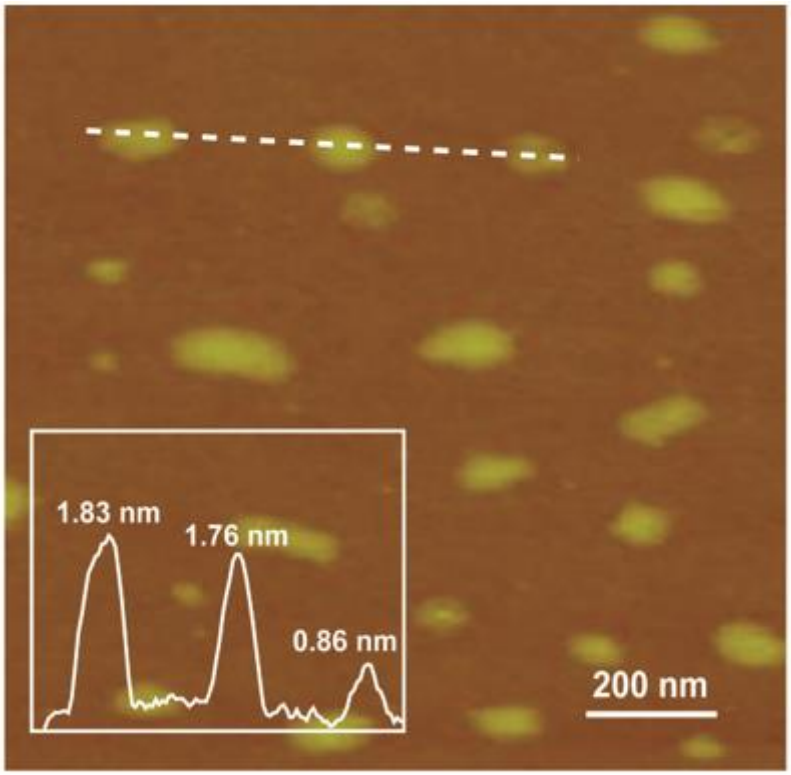

Figure 2.5 AFM image of WSe_2 flakes. The inset represents the height profile of the dotted region.

2.3 Surface Morphology of WSe_2-mediated PEDOT:PSS

Next, the surface morphology of WSe_2 added PEDOT:PSS film with various mixing ratio was characterized with scanning electron microscopy (SEM). As shown in Figure 2.6, SEM images show that the WSe_2-mediated PEDOT:PSS fully covered the ITO electrode without pin-holes along with no significant changes in the surface morphology with low concentration of WSe_2 (PEDOT:PSS to WSe_2 mixing ratio of 9:1, 3:1, v/v, henceforth denoted as P9, P3-WSe_2). Although, some WSe_2 flakes are observed, however, as shown in Figure 2.5, flakes were effectively exfoliated and expected to will not have a significant effect on the device performance. However, at the high concentration of WSe_2 (PEDOT:PSS to WSe_2 mixing ratio of 1:1, denoted as P1-WSe_2), flakes aggregated and formed a bulk state which can adversely affect the operation of device by disturbing the formation of photoactive layer and transport of photogenerated charge carriers at active layer.

To further investigate the effect of WSe_2 addition in PEDOT:PSS on surface morphology of HTL, the AFM analysis was additionally performed. As we expected in Figure 2.7, there was no changes in in film roughness with low concentration of WSe_2 addition. However, with the formation of WSe_2 aggregate at high concentration of WSe_2 addition, the surface roughness was increased about 4 times higher than that of pristine PEDOT:PSS. Along with SEM analysis, we could expect that the device performance will suffer from charge transporting the generated charge with P1-Wse_2 HTL.

2.4 Photovoltaic Performances of Organic Solar Cells

The device was fabricated to investigate the effect of WSe_2-modified PEDOT:PSS HTL in device performance. The conventional structured OSCs were fabricated by using poly[[4,8-bis[(2-ethylhexyl)oxy]benzo[1,2-b:4,5-b']dithiophene-2,6-diyl][3-fluoro-2-[(2-ethylhexyl)carbonyl]thieno[3,4-b]thiophenediyl]] (PTB7) as a donor and [6,6]-phenyl-C71-butyric acid methyl ester ($PC_{71}BM$) as a acceptor in photoactive layer. Details on device fabrication are provided in the Experimental Section. The current density-voltage characteristic under AM 1.5G illumination with 100 mW cm^{-2} irradiance are shown in Figure 2.8. And the corresponding photovoltaic parameters are summarized in Table 1. In Figure 2.8, we could observe remarkable improvement in the device performance was observed from the P3-WSe_2 device compare with PEDOT:PSS device, with the PCEs of 8.5% and 7.3%, respectively. P9-WSe_2 device also showed improvement (PCE = 7.8%). The improvement of device performance was mainly originated from enhanced current density (*Jsc*) and fill factor (FF). However, unlike the P9 and P3-WSe_2 device, the P1-WSe_2 device exhibit much lower device performance than PEDOT:PSS only device.

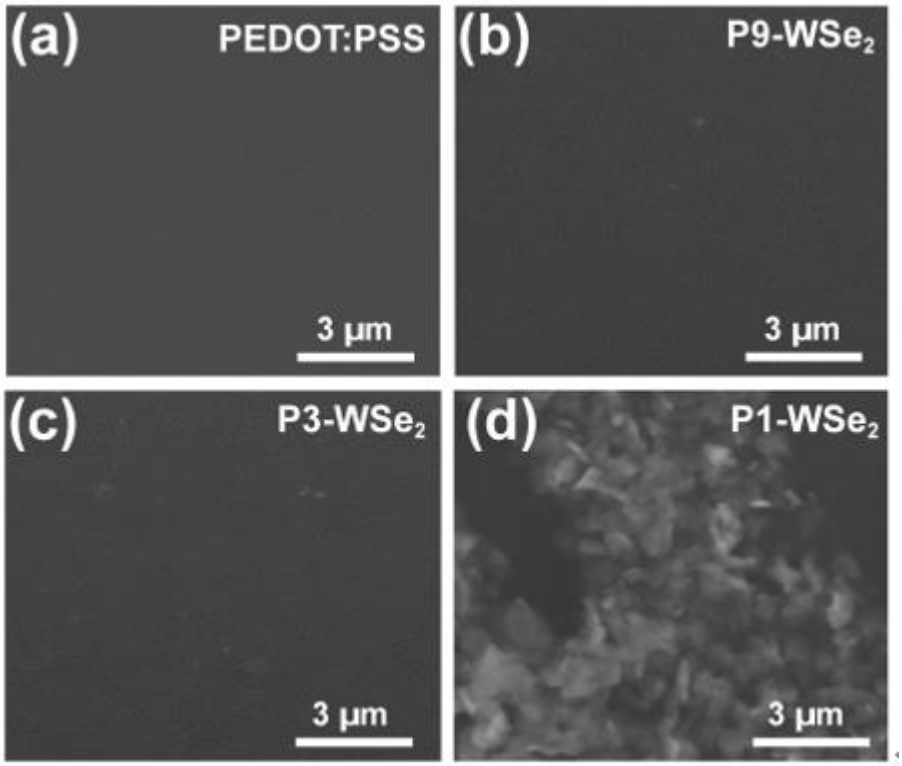

Figure 2.6 Surface morphology characterization of WSe_2-mediated PEDOT:PSS films. SEM images of (a) PEDOT:PSS, (b) P9-WSe_2, (c) P3-WSe_2, and (d) P1-WSe_2.

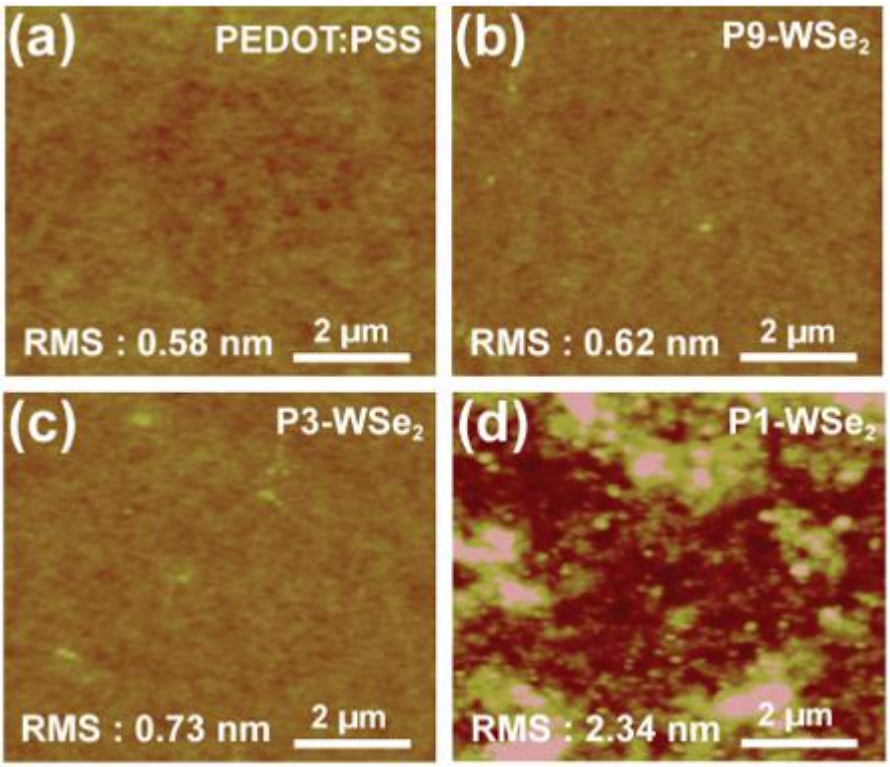

Figure 2.7 AFM topography images of (e) PEDOT:PSS, (f) P9-WSe_2, (g) P3-WSe_2, and (h) P1-WSe_2.

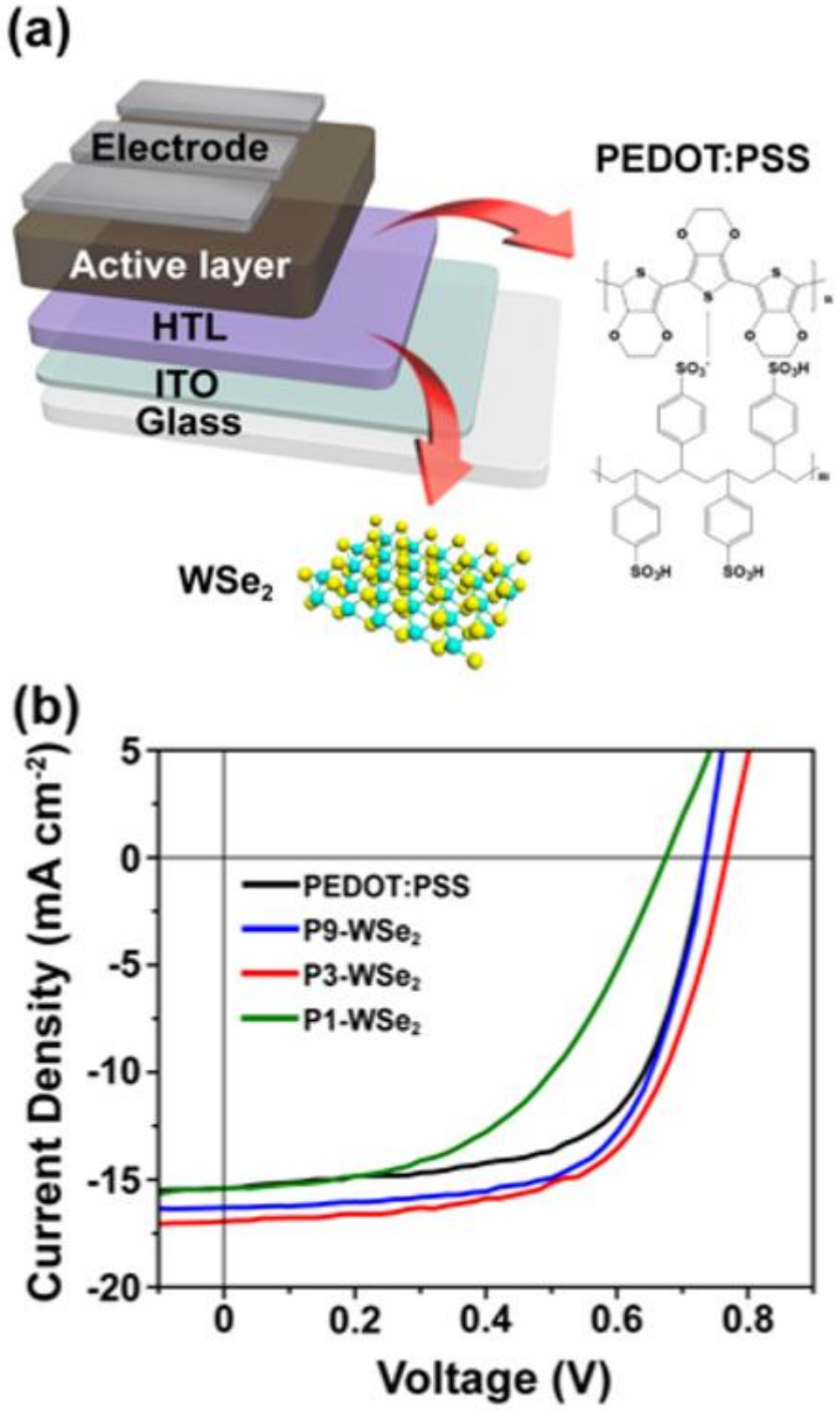

Figure 2.8 Device performance of PTB7:$PC_{71}BM$-based OSCs with WSe_2-mediated PEDOT:PSS HTL. (a) Schematic of the completed device structure. (b) $J-V$ characteristics.

Table 1. Device performance parameters of PTB7:$PC_{71}BM$-based conventional structured OSCs with varying WSe_2 concentrations in PEDOT:PSS.

HTL	J_{sc} [mA cm^{-2}]	V_{oc} [V]	FF [%]	PCE [%]
PEDOT:PSS	15.5 (15.3 ± 0.22)	0.76 (0.74 ± 0.01)	62.1 (62.0 ± 0.1)	7.3 (7.1 ± 0.1)
P9-WSe_2	16.1 (16.2 ± 0.14)	0.76 (0.75 ± 0.01)	63.8 (63.3 ± 0.1)	7.8 (7.7 ± 0.1)
P3-WSe_2	16.6 (16.6 ± 0.10)	0.78 (0.77 ± 0.01)	65.5 (65.3 ± 0.1)	8.5 (8.3 ± 0.1)
P1-WSe_2	15.3 (15.2 ± 0.26)	0.67 (0.65 ± 0.02)	48.9 (48.8 ± 0.3)	5.0 (4.6 ± 0.3)

To further investigate the reason for large decrease in device performance, we carried out photoluminescence (PL) analysis with various HTL. When the photogenerated charge carriers in photoactive layer recombined with each other, a PL peak generated, and when the charge carriers effectively extracted from the active layer to corresponding electrode, the associated PL peak quenches. As shown in Figure 2.9, since the charge recombination appeared immediately after exciton dissociation at the interface between donor and acceptor in the active layer, some PL peak was also observed with pristine PEDOT:PSS HTL. As expected in device performance, the decrease in PL peak is observed from P9 and P3-WSe_2 HTL compare to PEDOT:PSS indicating that the charge recombination in P9, P3-WSe_2 device was diminished and WSe_2-mediated PEDOT:PSS effectively extract the charge carriers from the active layer to electrode. However, with P1-WSe_2, enlarged PL intensity compare to pristine PEDOT:PSS was observed which indicates pronounced charge recombination. The increased recombination with P1-WSe_2 HTL might be associated with the relatively rough surface morphology of the film which is play as trap site within the charge transport. Thus, we could verify that the reason for deterioration in P1-WSe_2 device was increased charge recombination at the interface between active layer and HTL.

Before investigating the effect of WSe_2 addition into PEDOT:PSS and device performance, we first examine the effect of the solvent of WSe_2 dispersion in PEDOT:PSS. In previous studies, organic solvents, such as methanol, ethanol and dimethyl sulfoxide were added into PEDOT:PSS to increase the conductivity of PEDOT:PSS and PCE of devices by inducing phase separation between PEDOT and PSS and leading to larger domains with better connected PEDOT.[16-18] They showed that the highly hydrophilic solvents, with a high dielectric constant interact with the hydrophilic PSS and resulting in screening effect between PEDOT and PSS. To determine whether the improved device performance is due to water and IPA, we compare the PEDOT:PSS only device and co-solvent added PEDOT:PSS device (Figure 2.10). However, through the J-V curve and device parameters, we could verify that the there was almost no changes in device performance with co-solvent added PEDOT:PSS device which indicate that the solvent of WSe_2 dispersion have no effect on device efficiency. Since organic solvents can induce the phase separation between PEDOT:PSS, however, the solvent of WSe_2 solution did not appear to have a significant effect on PEDOT:PSS as the ratio of added solvent was very small compare to previous studies.

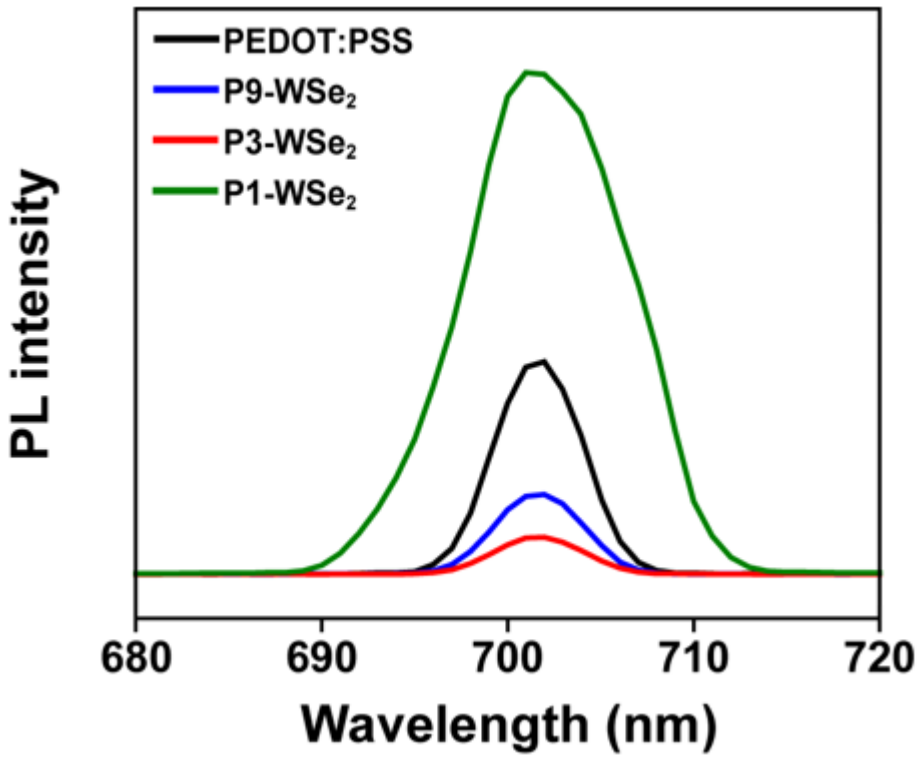

Figure 2.9 Steady state PL spectra measured from the structure of glass/PEDOT:PSS or P-WSe_2/PTB7:$PC_{71}BM$.

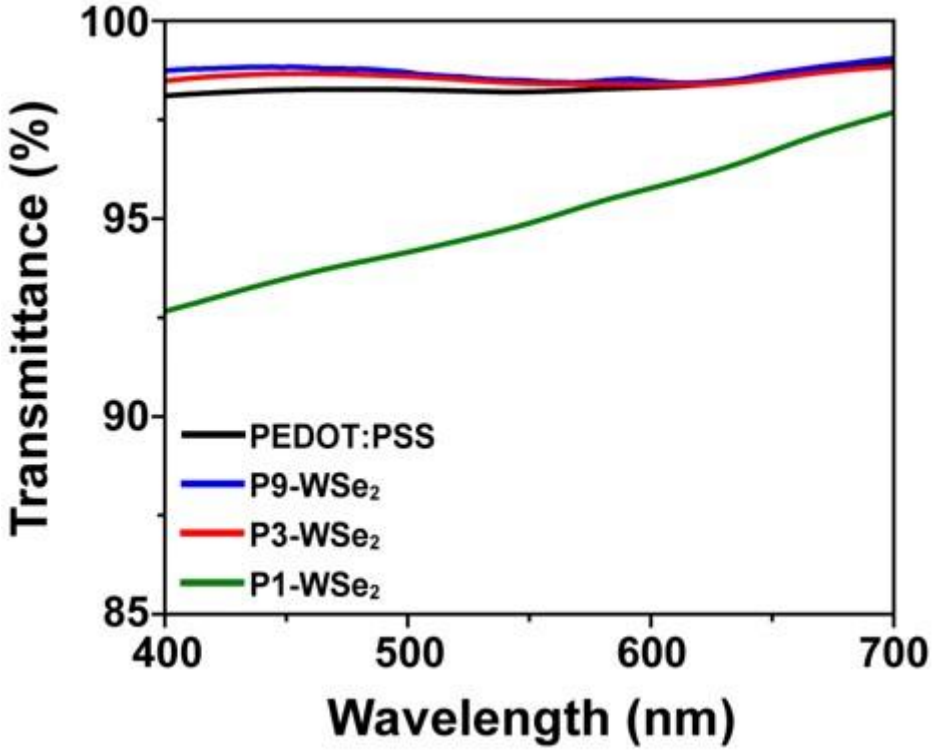

Figure 2.10 Device performance of OSCs with PEDOT:PSS and co-solvent(water/IPA) added PEDOT:PSS HTL. The mixing ratio between PEDOT:PSS and co-solvent was 3:1.

Table 2. Device performance parameters of PTB7:$PC_{71}BM$-based conventional structured OSCs with pristine PEDOT:PSS and co-solvent added PEDOT:PSS.

HTL	J_{sc} [mA cm^{-2}]	V_{oc} [V]	FF [%]	PCE [%]
PEDOT:PSS	15.5 (15.3 ± 0.22)	0.76 (0.74 ± 0.01)	62.1 (62.0 ± 0.1)	7.3 (7.1 ± 0.1)
PEDOT:PSS + water/IPA	15.7 (15.6 ± 0.21)	0.76 (0.75 ± 0.01)	62.3 (62.1 ± 0.1)	7.4 (7.1 ± 0.1)

2.5 Characterization of WSe_2-mediated PEDOT:PSS

As the WSe_2 solution was introduced into PEDOT:PSS solution for modification, the concentration of HTL could be diluted which can result in variation of film thickness and transmittance of HTL film. The transmittance of the HTL film play crucial role for device performance as it can affect the amount of light that reaches to photoactive layer and absorbed to generate charge carriers. Thus, we carried out the optical transmittance analysis of HTL film with various ratio of WSe_2 to investigate the reason for improved device performance in P9 and P3-Wse_2 device. As shown in Figure 2.11, we could confirm that there was no significant difference between pristine PEDOT:PSS and P9 and P3-WSe_2 HTL which implies that the increased current density and device performance was not originated from the difference in amount of absorbed light in photoactive layer. However, the large decrease in film transmittance was observed for P1-WSe_2 HTL. Despite the most diluted concentrations of HTL, the large decrease in film transmittance was probably due to the agglomerated WSe_2 flakes, as seen in surface morphology results. With these results, we could verify that the improved device performance of P9 and P3-WSe_2 performance was not from the difference in film transmittance and the deterioration of P1-WSe_2 device was may come from not only surface roughness but reduced film transmittance.

To further verify the reason for enhancement of WSe_2 modified PEDOT:PSS device, we characterized the work function of HTLs (Figure 2.12). With the suitable energy level of HTLs, the recombination of charge carriers at the interface between active layer and HTL can be suppressed by reducing the energy barrier between active layer and counter electrode which also resulting in improved device operations. As the work function of PEDOT:PSS is located at below the occupied molecular orbital of the donor, PTB7, where the generated hole moves, the generated charge may suffer some difficulty transport the hole. Thus, we verify the work function changes of HTL after WSe_2 addition. However, there was no significant changes in work function of modified HTL regardless of the mixing ration of WSe_2. The almost unchanged work function of HTL is probably due to the very small amount of added WSe_2 flakes despite of large difference in work function between PEDOT:PSS and WSe_2.[32] Although the increased work function with P3 and P1-WSe_2 PEDOT:PSS can promote the charge transport to electrode with favorable energy level alignment,[33-35] the improved device performance was may not the mainly comes from the work function changes.

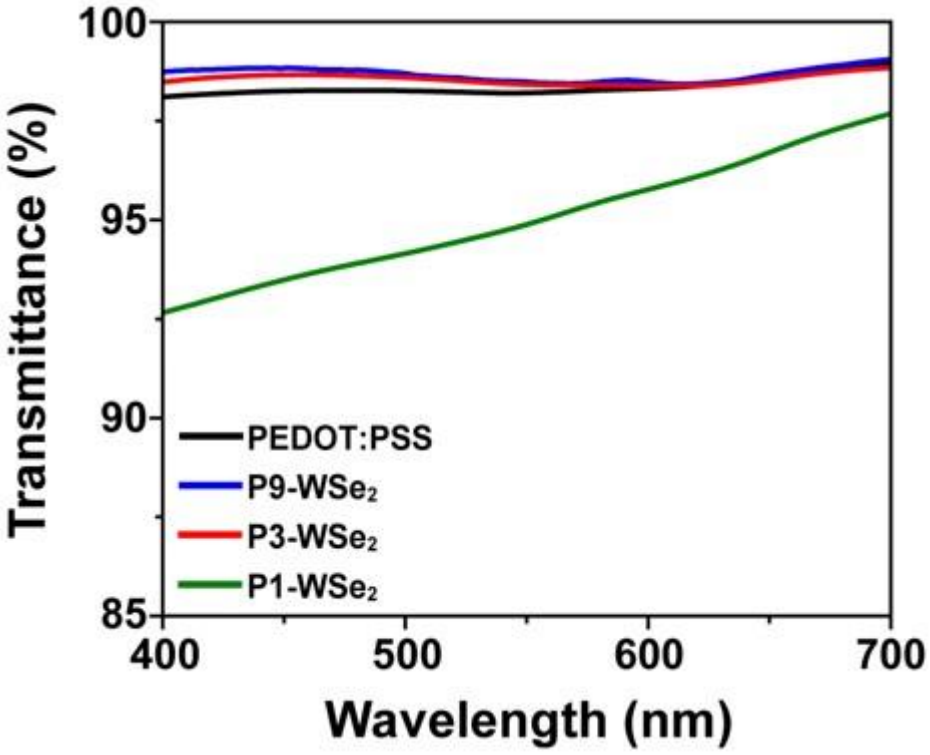

Figure 2.11 Optical transmittance of PEDOT:PSS and P-WSe_2 films.

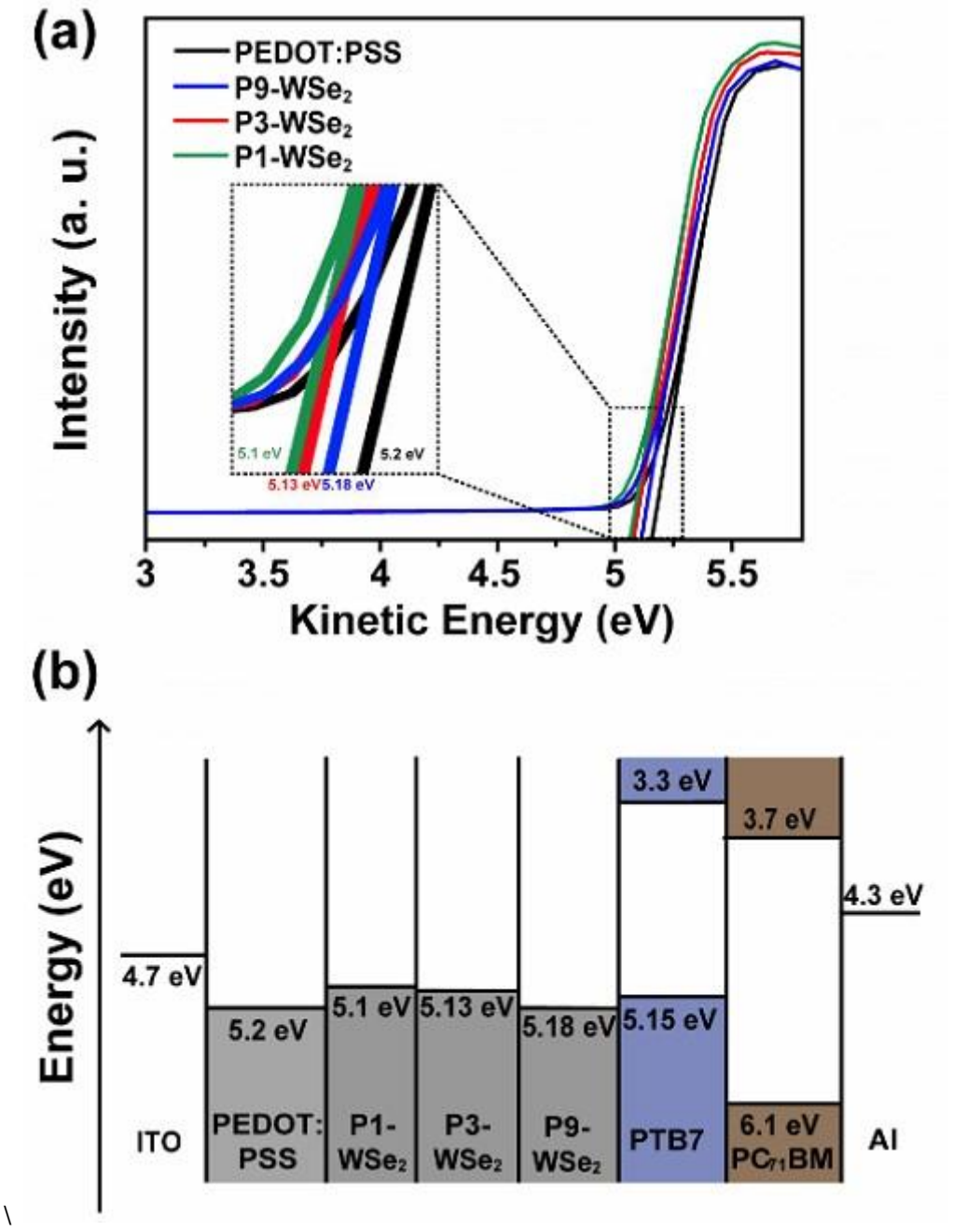

Figure 2.12 Work function of PEDOT:PSS and WSe_2-mediated PEDOT:PSS (a)UPS spectra from pristine PEDOT:PSS and WSe_2-mediated PEDOT:PSS. The inset present the enlargement of the cut-off region. (b) The flat-band energy level diagram of the completed device with various HTL.

X-ray photoelectron spectroscopy (XPS) characterization was performed to further investigate the effect of WSe_2 addition in the chemical composition of PEDOT:PSS. In Figure 2.13, the XPS spectra of S 2p from pristine PEDOT:PSS exhibit two dominant peaks at binding energies of 168.6 eV and 164.8 eV. Two distinct peaks were attributed to the thiophene and sulfonate units in PEDOT and PSS, respectively.[36,37]In pristine PEDOT:PSS, the conducting PEDOT polymer and insulating PSS polymer are attached to each other via very weak Coulombic interaction. PSS polymer was used to disperse PEDOT in water solvent, however, insulating property of PSS hindered the conductivity of PEDOT:PSS film which result in impediment of the device performances. However, after addition of WSe_2 into PEDOT:PSS, we observe that the ratio of PSS to PEDOT gradually decreased from 6.25 with pristine PEDOT:PSS to 4.54, 3.84 and 3.83 with P9, P3, P1-WSe_2, respectively. The decreased ratio of PSS to PEDOT implies that the WSe_2 additive in PEDOT:PSS induces a phase separation between PEDOT and PSS and aggregation of conducting PEDOT after adding the WSe_2 solutions into PEDOT:PSS. With formation of PEDOT aggregation which has conducting property, the modified HTL was expected to provide more efficient pathway for the generated charge carriers to reach the electrode and have improved hole transport ability.

To find out the reason for phase separation between PEDOT and PSS, we further investigate the WSe_2 flakes. To separate PEDOT and PSS, the weak coulombic interaction between PEDOT and PSS need to be broken caused by a specific charge. The Zeta potential measurement were carried out to investigate the surface charge of WSe_2 flakes. As shown in Figure 2.14, the zeta potential results exhibit the negatively charge distribution of WSe_2 flakes which indicate that the most of WSe_2 flakes have negatively charged surface. With the surface charge of WSe_2, the incorporated WSe_2 flakes in PEDOT:PSS may weaken the Coulombic interaction between PEDOT and PSS resulting in phase separation between two polymers and aggregation of PEDOT around the WSe_2 flakes.[27] The gradually decreased ratio of PSS to PEDOT in XPS results was comes from the phase separation between PEDOT and PSS and aggregation of PEDOT polymer around the WSe_2 which caused by negatively charged surface of WSe_2 flakes.

We further confirmed the conductivity of PEDOT:PSS and P3-Wse_2 HTL films to verify the separation of PEDOT and PSS by surface charge of WSe_2. By conformation changes from a coiled structure to extended-coil structure of PEDOT, the conductivity also enhanced to 1.1×10^{-2} S/cm from 6.02×10^{-3} S/cm of the pristine PEDOT:PSS as we expected from device performance and XPS results (Figure 2.15).

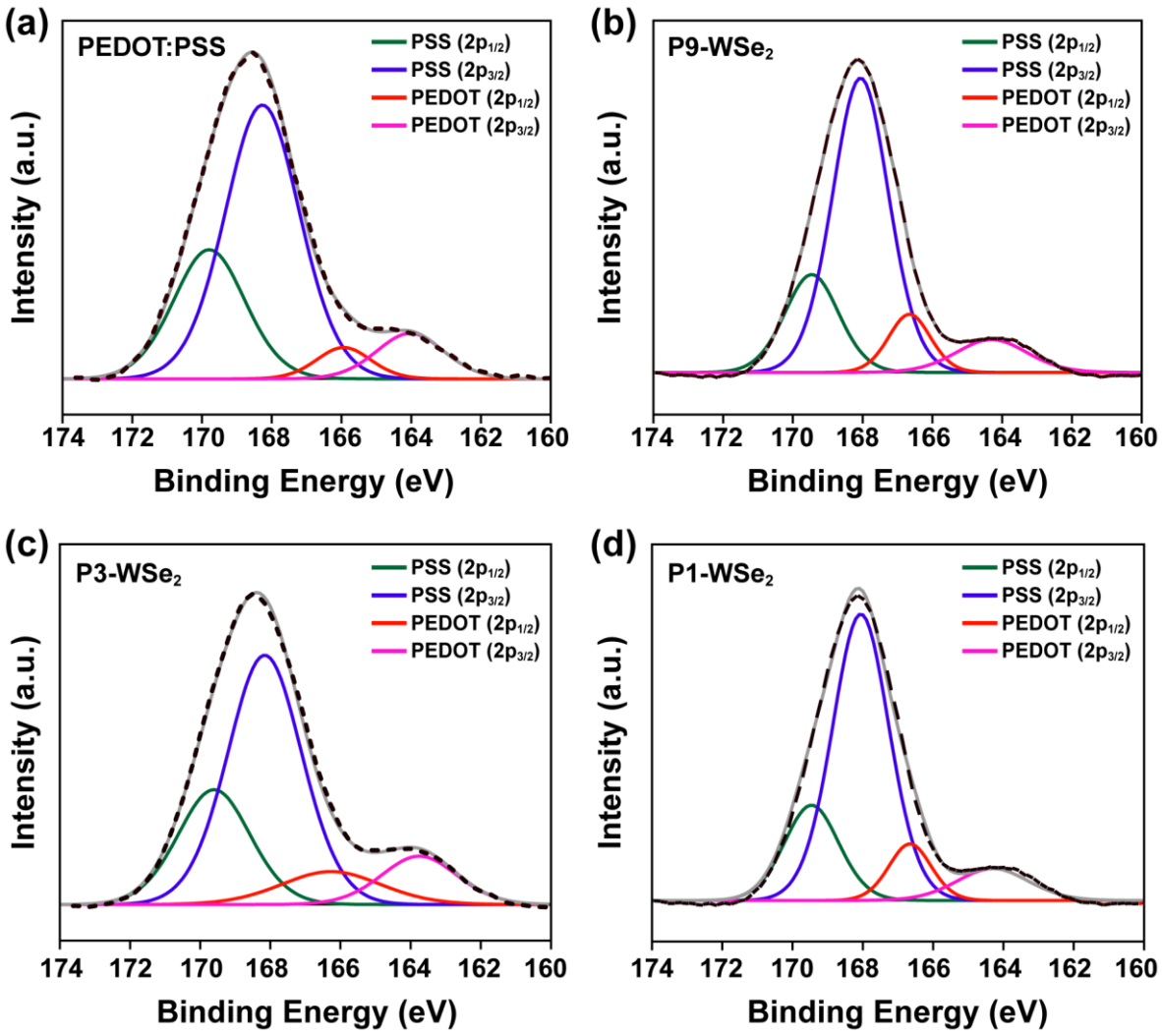

Figure 2.13 Chemical composition analysis of WSe_2-mediated PEDOT:PSS. XPS spectra of S 2p from (a) PEDOT:PSS, (b) P9-WSe_2, (c) P3-WSe_2, and (d) P1-WSe_2. The dashed black and solid gray lines represent the fitted profile and raw data, respectively.

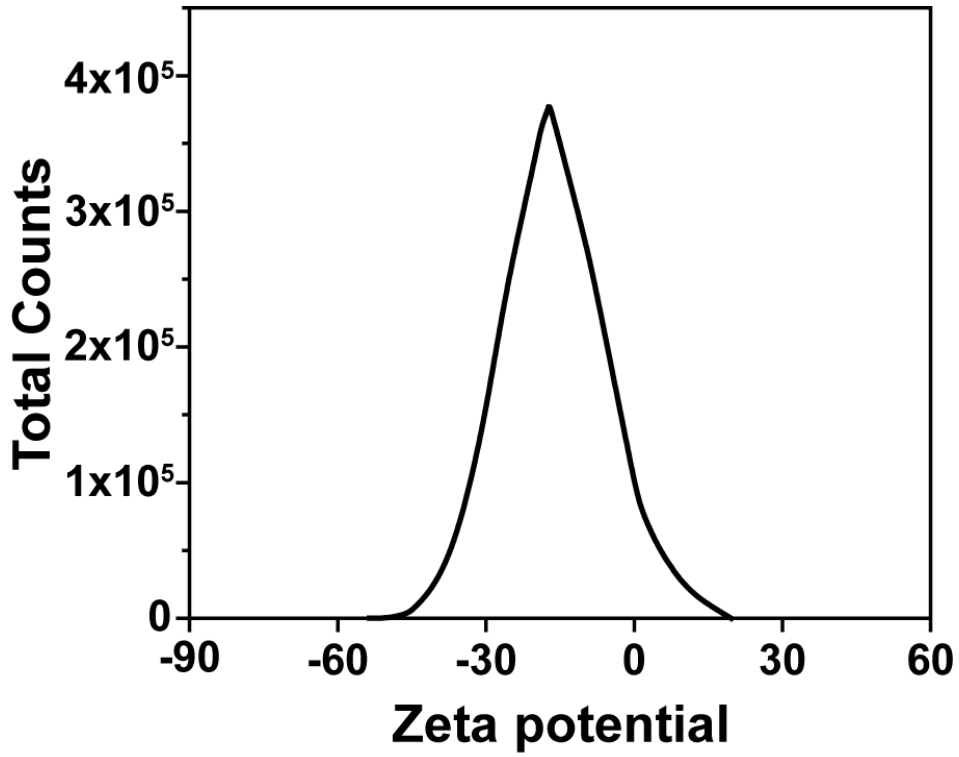

Figure 2.14 Zeta potential distribution of WSe_2.

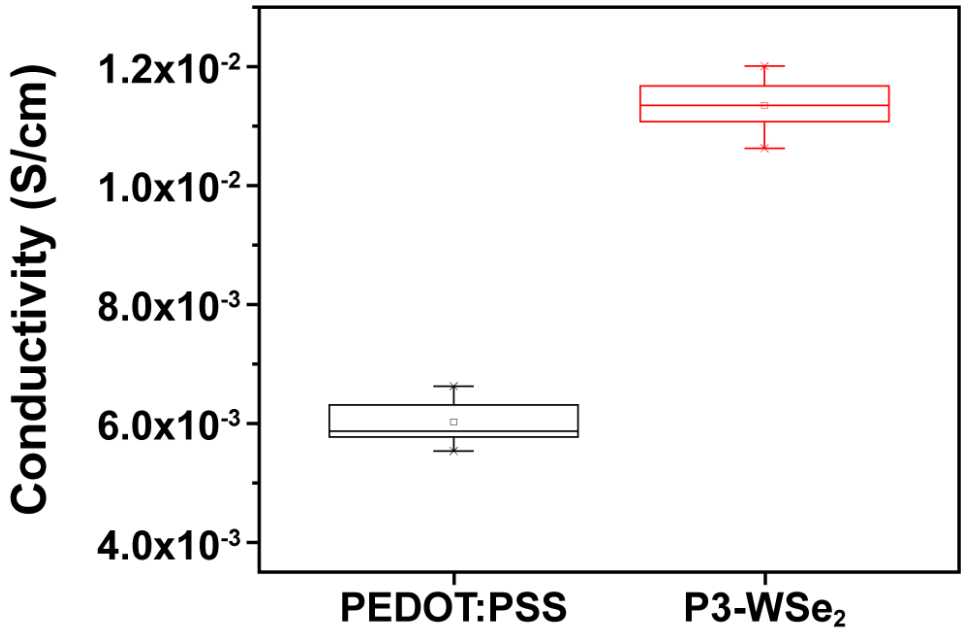

Figure 2.15 Comparison of conductivity between PEDOT:PSS and P3-WSe_2 film.

2.6 Charge Dynamics of completed device

To investigate the relationship between the enhanced conductivity and the charge transport ability of WSe_2-mediated PEDOT:PSS, we performed the charge transport and recombination dynamics of WSe_2-mediated PEDOT:PSS device, *Jsc* and *Voc* dependence on light intensity (I), charge transport resistance, photocurrent, and hole mobility measurements were performed on the best performing P3-WSe_2 device. The light intensity dependence of *Jsc* follows the power law described as $J_{sc} \propto I^{\alpha}$, where α is the coefficient of the power law.[38,39] As shown in Figure 2.16a, the increased value of α, with P3-WSe_2 (α = 0.99) device implies better charge extraction with reduced bimolecular recombination compared to the pristine PEDOT:PSS device (α = 0.97), which is reflected in the *Jsc* enhancement. In open-circuit condition, *Voc* varies with light intensity by the following relation, $V_{oc} \propto (kT/q) \ln I$. As shown in Figure 2.16b, the lower slope from P3-WSe_2 device also corroborates the suppressed bimolecular recombination with WSe_2-mediated PEDOT:PSS layer. Furthermore, electrochemical impedance spectroscopy (EIS) measurement was performed to examine the interfacial charge transport at the HTL, and the associated Nyquist plots of PEDOT:PSS and P3-WSe_2 films are presented in Figure 2.17. The lower transport resistance (R_{tr}) in P3-WSe_2 (243.9 Ω) than that of PEDOT:PSS (541.3 Ω) also indicates enhanced charge transporting efficiency at the junction interface, which supports the improvement of overall solar cell performance from the P3-WSe_2 device. Enhanced charge collection from the modified HTL can also be observed from the photocurrent density versus effective voltage ($J_{ph} - V_{eff}$) measurements (Figure 2.18), where $J_{ph} = J_L - J_D$ (J_D and J_L are the current densities under dark and illuminated conditions, respectively) and $V_{eff} = V_0 - V$ (V_0 is the voltage when J_{ph} is zero and V is the applied bias across the device). The higher saturated J_{ph} with P3-WSe_2 film indicates the improved charge transport ability of the WSe_2-mediated HTL, leading to the enhanced current density.[40] To further examine the charge transport ability between the anode and the photoactive layer, the hole mobilities of pristine and WSe_2-mediated PEDOT:PSS films were evaluated using the space charge-limited current (SCLC) model from the Mott-Gurney theory, $J = \frac{9}{8}\varepsilon_0\varepsilon_r\mu\frac{V^2}{d^3}$, where $\varepsilon_0\varepsilon_r$ is the dielectric constant of photoactive material, μ is the mobility, d is thickness of the photoactive layer, and V is the voltage across the device. The hole-only device was fabricated with the structure of glass/ITO/PEDOT:PSS or P3-WSe_2/PTB7:$PC_{71}BM$/MoO_3/Au. As shown in Figure 2.19, enhanced hole current density from the P3-WSe_2 device compared with that from the PEDOT:PSS only device, with estimated hole mobilities of 7.8×10^{-6} and 1.5×10^{-6} cm2 $V^{-1}s^{-1}$, respectively, implies efficient hole transport and enhanced extraction efficiency, corresponding to the improvement of *Jsc* in overall device performance.[41,42]

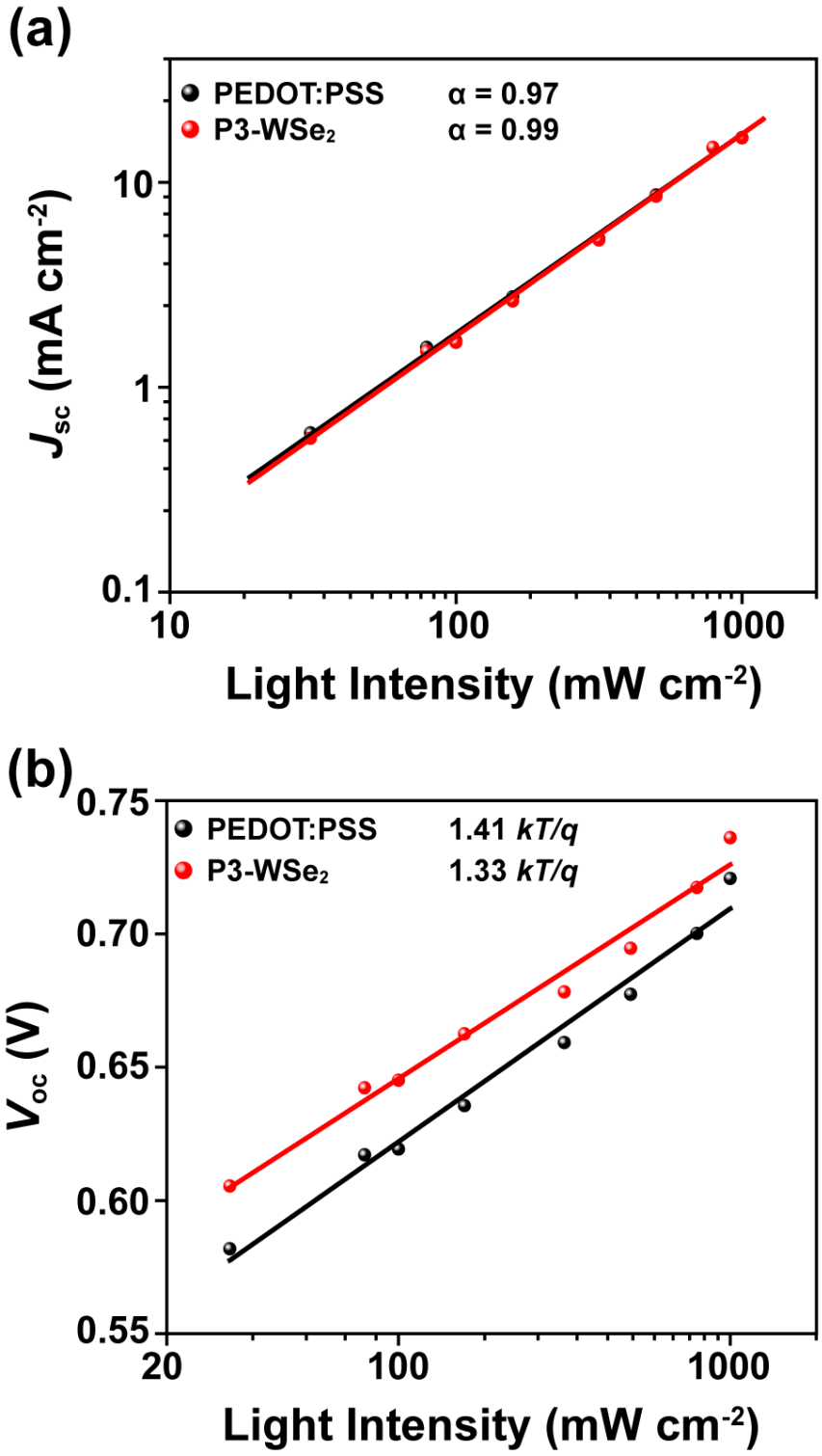

Figure 2.16 Charge dynamics analysis of completed devices with different HTL configurations. Light intensity dependent (a) J_{sc} and (b) V_{oc}.

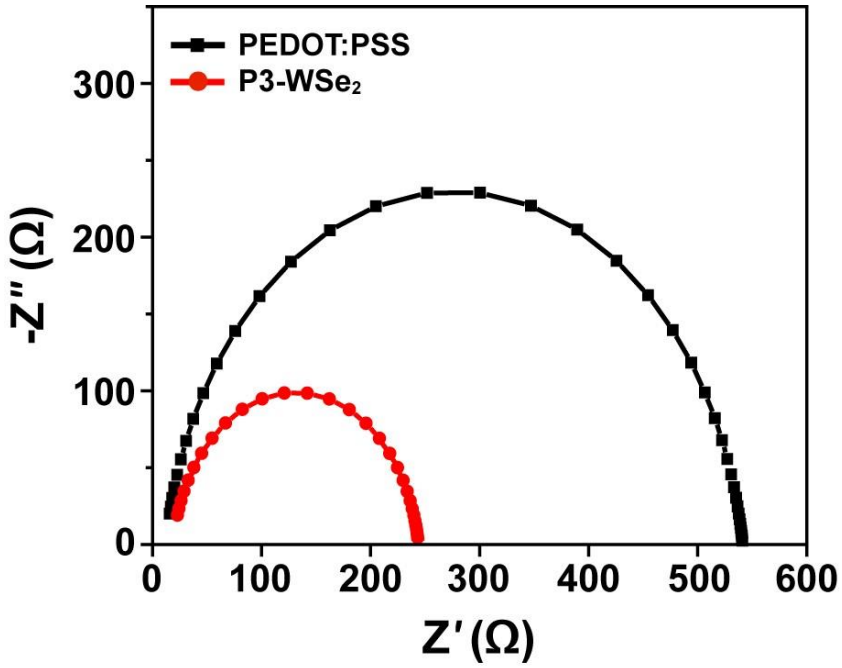

Figure 2.17 Nyquist plot of HTL films with PEDOT:PSS and P3-WSe_2. The inset diagram describes the schematic of the equivalent circuit model.

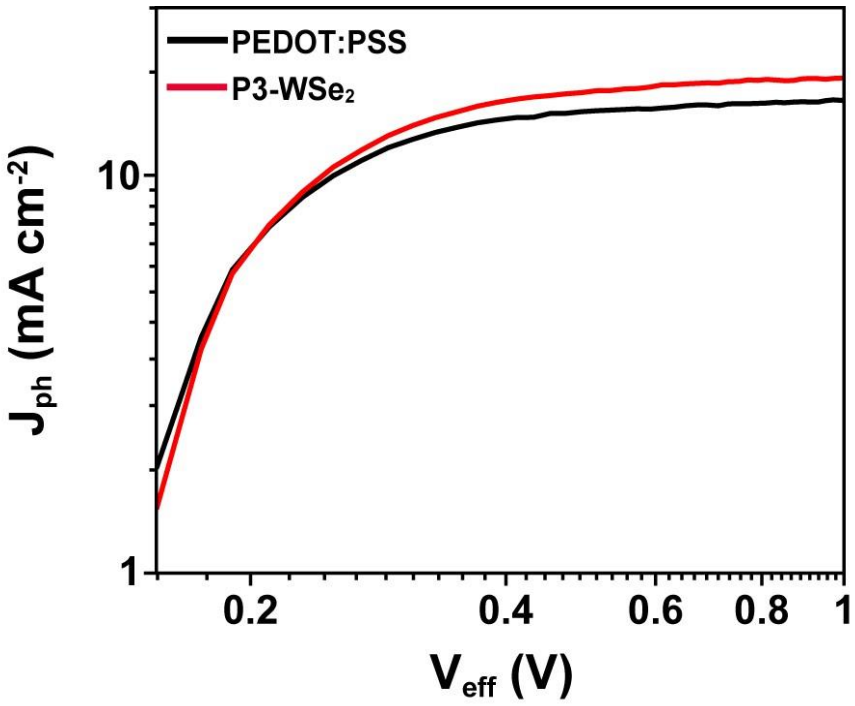

Figure 2.18 Photocurrent density versus effective voltage characteristics.

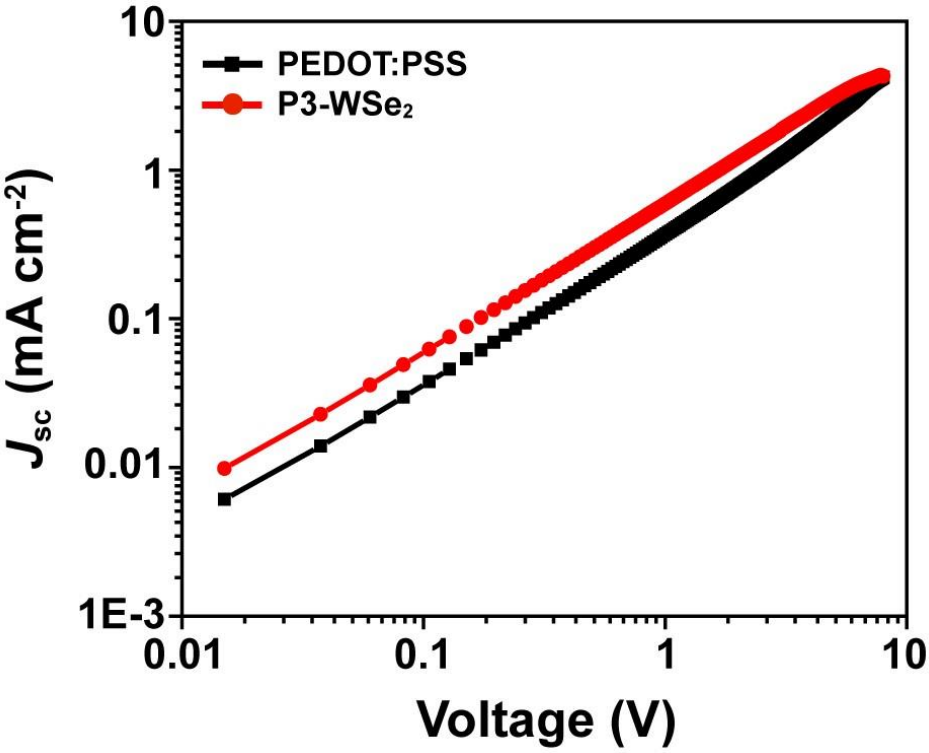

Figure 2.19 *J*−*V* characteristics of hole-only devices by space-charge-limited current method.

III. Conclusion

In this study, we successfully developed a facile strategy to enhance the device performance of OSCs by modifying the charge transporting material with TMDs. Addition of WSe_2 into PEDOT:PSS resulted in notable improvement of PCE from 7.3% to 8.5% at optimized conditions. The enhancement of device performances is mainly attributed to the improved hole transport ability through WSe_2-mediated PEDOT:PSS HTL layer. Negatively charged surface of WSe_2 weakens the Coulombic interaction between PEDOT and PSS, triggering the phase separation of PEDOT and PSS, which provides efficient pathways for the photogenerated charge carriers. The reduction of charge transport resistance and charge recombination loss were also verified from the charge dynamics analysis. This work demonstrates a promising approach to improve the hole transporting ability of the HTL in OSCs toward enhanced device performance, which may broaden the application of TMDs in various optoelectronic devices beyond the solar cells

IV. Experimental Section

Exfoliation of WSe_2

Bulk WSe_2 powder (10 μm, purity>99.8%) was purchased from Alfa Aesar and used as-received. For the preparation of WSe_2 flakes, 100 mg of WSe_2 powders were dispersed in 20 mL co-solvent of water and IPA mixture with the optimized ratio of 4:6 (water:IPA, v/v), which was exfoliated via tip sonicator (Sonic & materials, VC 505). The solution was centrifuged and the supernatant was collected for further analysis and device fabrication. The final concentration of optimized WSe_2 dispersion from the co-solvent mixture of 4:6 was 0.9 mg/mL.

Solar cell fabrication

OSCs were fabricated with the structure of glass/ITO/HTL/PTB7:$PC_{71}BM$/Al. ITO-coated glass were cleaned using sonication in deionized water, acetone, and isopropyl alcohol, followed by O_2 plasma treatment. PEDOT:PSS and P-WSe_2 solution was spin-coated on ITO substrate at 4000 rpm for 1 min and subsequently annealed at 120 °C for 10 min. PTB7 and $PC_{71}BM$ were dissolved in chlorobenzene:1,8-diiodooctane (97:3 vol%) with concentrations of 12 and 40 mg mL^{-1}, respectively. The blended solution was spin-coated at 900 rpm for 2 min. Finally, Al electrode was thermally evaporated with a thickness of 100 nm at base pressure of 2×10^{-6} Torr.

Measurements and Characterization

Absorption and transmittance measurements were performed using UV−Vis−NIR spectrophotometer (Cary 5000, Agilent). Raman spectroscopy was conducted by confocal Raman (alpha300R, WITec). J−V characteristics were measured under AM 1.5G illumination using Xenon arc lamp solar simulator w ith Keithley 2635A source meter. Steady state photoluminescence was measured by fluorescence spect rometer (NF900, Edinburgh Instrument). Tapping mode AFM (DI-3100, Veeco) and SEM (S-4800, Hitachi) were used to analyze the surface morphology. XPS and UPS spectra were obtained usi ng ESCALAB 250XI (Thermo Fisher Scientific). Surface charge distribution of WSe_2 was examined by Zeta sizer (Nano ZS, Malvern). EIS measurement was carried out by impedance analyzer (SI1260, Solartron). Neutral density filters were used to measure the light intensity dependent *Jsc* and *Voc*. Carr ier mobility was calculated from Mott-Gurney relation by fabricating the hole-only device with a structure of glass/ITO/HTL/PTB7:$PC_{71}BM$/MoO_3/Au.

References

(1) Sariciftci, N. S.; Smilowitz, L.; Heeger, A. J.; Wudl, F. Photoinduced Electron Transfer from a Conducting Polymer to Buckminsterfullerene. *Science* **1992**, *258*, 1474-1476.

(2) Yu, G.; Gao, J.; Hummelen, C.; Wudl, F.; Heeger, A. J. Polymer Photovoltaic Cells: Enhanced Efficiencies via a Network of Internal Donor-Acceptor Heterojunctions. *Science*, **1995**, *270*, 1789-1791.

(3) Park, S. H.; Roy, A.; Beaupré, S.; Cho, S.; Coates, N.; Moon, J. S.; Moses, D.; Leclerc, M.; Lee, K.; Heeger, A. J. Bulk heterojunction solar cells with internal quantum efficiency approaching 100%. *Nat. Photonics* **2009**, *3*, 297-302.

(4) Peters, C. H.; Sachs-Quintana, I. T.; Kastrop, J. P.; Beaupré, S.; Leclerc M.; McGehee, M. D. High Efficiency Polymer Solar Cells with Long Operating Lifetimes. *Adv. Energy Mater.* **2011**, *1*, 491-494.

(5) Yang, Y.; Chen, W.; Dou, L.; Chang, W.-H.; Duan, H.-S.; Bob, B.; Li, G.; Yang, Y. High-performance multiple-donor bulk heterojunction solar cells. *Nat. Photonics* **2015**, *9*, 190-198.

(6) Zhao, J.; Li, Y.; Yang, G.; Jiang, K.; Lin, H.; Ade, H.; Ma, W.; Yan, H. Efficient organic solar cells processed from hydrocarbon solvents. *Nat. Energy* **2016**, *1*, 15027.

(7) Chueh, C.-C.; Chien, S.-C.; Yip, H.-L.; Salinas, J. F.; Li, C.-Z.; Chen, K.-S.; Chen, F.-C.; Chen, W.-C.; Jen, A. K.-Y. Toward High-Performance Semi-Transparent Polymer Solar Cells: Optimization of Ultra-Thin Light Absorbing Layer and Transparent Cathode Architecture. *Adv. Energy Mater.* **2013**, *3*, 417-423.

(8) Wang, Y.; Tong, S. W.; Xu, X. F.; Özyilmaz, B.; Loh, K. P. Interface Engineering of Layer-by-Layer Stacked Graphene Anodes for High-Performance Organic Solar Cells. *Adv. Mater.* **2011**, *23*, 1514-1518.

(9) Jung, S.; Lee, J.; Seo, J.; Kim, U.; Choi Y.; Park, H. Development of Annealing-Free, Solution-Processable Inverted Organic Solar Cells with N-Doped Graphene Electrodes using Zinc Oxide Nanoparticles. *Nano Lett.* **2018**, *18*, 1337-1343.

(10) He, Z.; Zhong, C.; Su, S.; Xu, M.; Wu, H.; Cao, Y. Enhanced power-conversion efficiency in polymer solar cells using an inverted device structure. *Nat. Photonics* **2012**, *6*, 591-595.

(11) Loser, S.; Valle, B.; Luck, K. A.; Song, C. K.; Ogien, G.; Hersam, M. C.; Singer, K. D.; Marks, T. J. High-Efficiency Inverted Polymer Photovoltaics via Spectrally Tuned Absorption Enhancement. *Adv. Energy Mater.* **2014**, *4*, 1301938.

(12) Park, K. H.; An, Y.; Jung, S.; Park, H.; Yang, C. Locking-In Optimal Nanoscale Structure Induced by Naphthalenediimide-Based Polymeric Additive Enables Efficient and Stable Inverted Polymer Solar Cells. *ACS Nano* **2017**, *11*, 7409-7415.

(13) Min, J.; Luponosov, Y. N.; Cui, C.; Kan, B.; Chen, H.; Wan, X.; Chen, Y.; Ponomarenko, S. A.; Li, Y.; Brabec, C. J. Evaluation of Electron Donor Materials for Solution-Processed Organic Solar Cells via a Novel Figure of Merit. *Adv. Energy Mater.* **2017**, *7*, 1700465.

(14) Yu, R.; Zhang, S.; Yao, H.; Guo, B.; Li, S.; Zhang, H.; Zhang, M.; Hou, J. Two Well-Miscible Acceptors Work as One for Efficient Fullerene-Free Organic Solar Cells. *Adv. Mater.* **2017**, *29*, 1700437.

(15) Kim, Y. H.; Sachse, C.; Machala, M. L.; May, C.; Müller-Meskamp, L.; Leo, K. Highly Conductive PEDOT:PSS Electrode with Optimized Solvent and Thermal Post-Treatment for ITO-Free Organic Solar Cells. *Adv. Funct. Mater.* **2011**, *21*, 1076-1081.

(16) Kee, S.; Kim, N.; Kim, B. S.; Park, S.; Jang, Y. H.; Lee, S. H.; Kim, J.; Kim, J.; Kwon, S.; Lee, K. Controlling Molecular Ordering in Aqueous Conducting Polymers Using Ionic Liquids. *Adv. Mater.* **2016**, *28*, 8625-8631.

(17) Alemu, D.; Wei, H.-Y.; Ho, K.-C.; Chu, C.-W. Highly conductive PEDOT:PSS electrode by simple film treatment with methanol for ITO-free polymer solar cells. *Energy Environ. Sci.* **2012**, *5*, 9662.

(18) Mengistie, D. A.; Wang, P.-C.; Chu, C.-W. Effect of molecular weight of additives on the conductivity of PEDOT:PSS and efficiency for ITO-free organic solar cells. *J. Mater. Chem. A* **2013**, *1*, 9907.

(19) Gu, X.; Cui, W.; Li, H.; Wu, Z.; Zeng, Z.; Lee, S.-T.; Zhang, H.; Sun, B. Solution-Processed Hole Extraction Layer Made from Ultrathin MoS_2 Nanosheets for Efficient Organic Solar Cells. *Adv. Energy Mater.* **2013**, *3*, 1262-1268.

(20) Gu, X.; Cui, W.; Song, T.; Liu, C.; Shi, X.; Wang, S.; Sun, B. Solution-Processed 2D Niobium Diselenide Nanosheets as Efficient Hole-Transport Layers in Organic Solar Cells. *ChemSusChem* **2014**, *7*, 416-420.

(21) Liu, X.; Kim, H.; Guo, L. J. Solution-Processed 2D Niobium Diselenide Nanosheets as Efficient Hole-Transport Layers in Organic Solar Cells. *Organ. Electron.* **2014**, *14*, 591-598.

(22) Li, S.-S.; Li, K.-H.; Lin, C.-C.; Chen, C.-W.; Chhowalla, M. Solution-Processable Graphene Oxide as an Efficient Hole Transport Layer in Polymer Solar Cells. *ACS Nano* **2010**, *4*, 3169-3174.

(23) Yang, X.; Fu, W.; Liu, W.; Hong, J.; Cai, Y.; Jin, C.; Xu, M.; Wang, H.; Yang, D.; Chen, H. Engineering crystalline structures of two dimensional MoS_2 sheets for high-performance organic solar cells. *J. Mater. Chem. A* **2014**, *2*, 7727.

(24) Le, Q. V.; Nguyen, T. P.; Kim, S. Y. UV/ozone-treated WS_2 hole-extraction layer in organic photovoltaic cells. *Phys. Status Solidi RRL 8*, **2014**, *5*, 390-394.

(25) Rafique, S.; Abdullah, S. M.; Shahid, M. M.; Ansari M. O.; Sulaiman, K. Significantly improved photovoltaic performance in polymer bulk heterojunction solar cells with graphene oxide/PEDOT:PSS double decked hole transport layer. *Sci. Rep.* **2016**, *7*, 39555.

(26) Iwan, A.; Caballero-Vriones, F.; Filapek, M.; Boharewicz, B.; Tazbir, I.; Hreniak, A.; Guerrero-Contrearas, J. Electrochemical and photocurrent characterization of polymer solar cells with improved performance after GO addition to the PEDOT:PSS hole transporting layer. *Sol. Energy* **2017**, *146*, 230-242.

(27) Dehsari, H. S.; Shalamzari, E. K.; Gavgani, J. N.; Taromi, F. A.; Ghanvary, S. Efficient preparation of ultralarge graphene oxide using a PEDOT:PSS/GO composite layer as hole transport layer in polymer-based optoelectronic devices. *RSC Adv.* **2014**, *4*, 55067.

(28) Dong, N.; Li, Y.; Feng, Y.; Zhang, S.; Zhang, X.; Chang, C.; Fan, J.; Zhang, L.; Wang, J. Optical Limiting and Theoretical Modelling of Layered Transition Metal Dichalcogenide Nanosheets. *Sci. Rep.* **2015**, *5*, 14646.

(29) Dong, N.; Li, Y.; Zhang, S.; Mcevoy, N.; Zhang, X.; Cui, Y.; Zhang, L.; Duesberg, G. S.; Wang, J. Dispersion of nonlinear refractive index in layered WS_2 and WSe_2 semiconductor films induced by two-photon absorption. *Opt. Lett.* **2016**, *41*, 3936-3939.

(30) Zeng, H.; Liu, G.-B.; Dai, J.; Yan, Y.; Zhu, B.; He, R.; Xie, L.; Xu, S.; Chen, X.; Yao, W.; Cui, X. Optical signature of symmetry variations and spin-valley coupling in atomically thin tungsten dichalcogenides. *Sci. Rep.* **2013**, *3*, 1608.

(31) Tonndorf, P.; Schmidt, R.; Böttger, P.; Zhang, X.; Börner, J.; Liebig, A.; Albrecht, M.; Kloc, C.; Gordan, O.; Zahn, D. R. T.; Vasconcellos, S. M.; Bratschitsh, R. Photoluminescence emission and Raman response of monolayer MoS2, MoSe2, and WSe2. *Opt. Express* **2013**, *21*, 4908-4916.

(32) Gong, C.; Zhang, H.; Wang, W.; Colombo, L.; Wallace, R. M.; Cho, K. Band alignment of two-dimensional transition metal dichalcogenides: Application in tunnel field effect transistors *Appl. Phys. Lett.* **2013**, 103, 053513.

(33) Lee, T.-W; Chung, Y. Control of the Surface Composition of a Conducting-Polymer Complex Film to Tune the Work Function *Adv. Funct. Mater*. **2008**, 18, 2246-2252.

(34) Nevrela, J.; Micjan, M.; Novota, M.; Kovacova, S.; Pavuk, M.; Juhasz, P.; Kovac, J.; Jakabovic, J.; Weis, M. Secondary doping in poly(3,4-ethylenedioxythiophene):Poly(4-styrenesulfonate) thin films *J. Polym. Sci., Part B: Polym. Phys.* **2015**, 53, 690-699.

(35) Shuttle, C. G.; O'Regan, B.; Ballantyne, A. M.; Nelson, J.; Bradley, D. D. C.' Durrant, J. R. Bimolecular recombination losses in polythiophene: Fullerene solar cells *Phys. Rev. B* **2008**, 78, 113201.

(36) Ouyang, J.; Chu, C.-W.; Chen, F.-C.; Xi, Q.; Yang, Y. High-Conductivity Poly(3,4-Ethylenedioxythiophene):Poly(styrenesulfonate) Film and Its Application in Polymer Optoelectronic Devices. *Adv. Funct. Mater.* **2005**, *15*, 203-208.

(37) Zotti, G.; Zecchin, S.; Schiavon, G.; Louwet, F.; Groenendaal, L.; Crispin, X.; Osikowicz, W.; Salaneck, W.; Fahlman, M. Electrochemical and XPS Studies toward the Role of Monomeric and Polymeric Sulfonate Counterions in the Synthesis, Composition, and Properties of Poly(3,4-ethylenedioxythiophene). *Macromolecules* **2003**, *36*, 3337-3344.

(38) Cowan, S. R.; Roy A.; Heeger, A. J. Recombination in polymer-fullerene bulk heterojunction solar cells. *Phys. Rev. B* **2010**, *82*, 245207.

(39) Hahn, T.; Tscheuschner, S.; Kahle, F.-J.; Reichenberger, M.; Athanasopouls, S.; Saller C.; Bazan, G. C.; Nguyen, T.-Q.; Strohriegl, P.; Bässler, H.; Köhler, A. Monomolecular and Bimolecular Recombination of Electron–Hole Pairs at the Interface of a Bilayer Organic Solar Cell. *Adv. Funct, Mater.* **2017**, *27*, 1604906.

(40) Huang, P.; Liu, Y.; Zhang, K.; Yuan, L.; Li, D.; Hou, G.; Dong, B.; Zhou, Y.; Song, B.; Li, Y. Catechol derivatives as dopants in PEDOT:PSS to improve the performance of p–i–n perovskite solar cells. *J. Mater. Chem. A* **2017**, *5*, 24275.

(41) Kim, G.-W.; Shinde, D. V.; Park, T. Thickness of the hole transport layer in perovskite solar cells: performance versus reproducibility. *RSC Adv.* **2015**, *5*, 99356.

(42) Li, Y.; Hong, N. An efficient hole transport material based on PEDOT dispersed with lignosulfonate: preparation, characterization and performance in polymer solar cells. *J. Mater. Chem. A* **2015**, *3*, 21537.

Acknowledgements

I would like to thank to my advisor, professor Heysung Park for giving me an opportunity to study in UNIST and insightful suggestion for my researches in master's course.

I also appreciate my committees of thesis, professor Changduk Yang and professor Jongnam Park who helped me to accomplish the thesis.

Finally, I would like to thank to Seungon Jung, Nam Khen Oh, Yunseong Choi, Jihyung Seo, Junghyun Lee, Ungsoo Kim who have characterized Raman, UV-vis-IR absorption, SEM, AFM, XPS, and Zeta potentials characterization in thesis.